ISSN 1 746-7233, England, UK
World Journal of Modelling and Simulation
Vol. 11 (2015) No. 1, pp. 69-80

Long endurance hybrid fuel cell-battery powered UAV

Karim N. Mobariz[1], Ahmed M. Youssef[1*], Mohamed Abdel-Rahman[2]

[1] Egyptian Armed Forces, Egypt
[2] Electrical Power Engineering, Ain Shams University, Egypt

(*Received October 2 2014, Accepted December 9 2014*)

Abstract. Unmanned aerial vehicles (UAVs) have gained much popularity in several military and civilian applications. Performing environmental monitoring, agriculture, and surveying applications have very specific constraints on power, cost, weight, and flight endurance. This paper presents the design of a renewable effective energy source for powering a long endurance UAV. This power unit consists of a fuel cell stack, a pack of Lithium-ion batteries, and a DC-DC buck converter. Designing the buck converter controller, and describing the interaction between the two sources of energy during operation of powering the propulsion system and the loads, are the main objectives of this paper.

Keywords: Unmanned aerial vehicle, polymer membrane fuel cell stack, battery, hybrid, buck converter

1 Introduction

Unmanned aerial vehicles (UAVs) have received considerable attention in many military and in law enforcement missions (e.g., reconnaissance, remote delivery of urgent equipment/material, battlefield monitoring, ordnance delivery, etc). UAVs have also gained popularity in civilian applications (crop spraying, geological surveying, search and rescue operations, etc). The reason for this attention is that UAV platforms are low-cost and viable alternatives to manned aircraft as valuable sources of data for much application. For UAVs to perform these long endurance applications, their power sources need to be developed to ensure the long endurance functionality of the propulsion system and onboard equipment[12].

The flight range of UAV is limited by the amount of fuel it carries. Increasing fuel will increase the total weight of the airplane, which in turn reduces the flight endurance. Although long endurance is achievable with conventional fuels, hydrocarbon-fueled systems are usually loud, inefficient, and unreliable when it comes to those small flying vehicles. On the other hand, batteries do not offer enough power for battery-powered systems for a long duration flight due to the low energy density of the battery system, especially where cameras and other equipment-powered by the same battery as the UAV's propulsive system-are in use. In addition to that, the longer battery charging time is another constraint to limit the pure battery driven vehicles. Therefore researchers started developing long endurance UAVs which rely on new effective sources of energy as their power sources. In addition to high efficiency, long endurance UAVs' power sources should possess the following properties: (1) high power and energy densities, and (2) fast dynamic response time in changes in power output[7]. Defining the following terms to be used throughout the paper; specific power and power density are the maximum available power that a source can deliver per unit weight (W/kg) and per unit volume (W/L), respectively, whilst specific energy and energy density are defined as the source's energy storage capacity per unit weight (Wh/kg) and per unit volume (Wh/L), respectively.

Consequently, many researchers are focused on the development of powering long endurance UAVs by renewable and clean energy sources. Alternatives to the combustion of gasoline and other fossil fuels,

* Corresponding author. *E-mail address*: ammyk_khater@yahoo.com.

renewable energy sources offer higher power and energy densities, lower cost, non-carbon emission, more-efficient power, lower acoustic and heat emissions which are also required to hinder detection and facilitate performing the missions. One of these renewable energy sources of electric power is the fuel cell.

In 2000, the United State National Research Council published a report describing the future research plan on UAV designs and propulsion technologies. This report showed the energy options for UAV power source with the flight duration[13]. A study on 60KW fuel cell powered aircraft propulsion system is conducted by NASA, in 2003[8]. One year later, a feasibility study about a fuel cell powered small scaled aircraft is published by Sehra et al.[17]. A conceptual design of a long endurance small scaled PEM fuel cell powered aircraft is revealed in Georgia Institute of Technology in 2006[5]. In 2009, the first commercial fuel cell powered UAV, named Boomerang is revealed[3]. In this year, a flight endurance of 26 hours was achieved by Ion Tiger from Naval Research Laboratory[2]. A funded project by the European commission for designing a fuel cell powered aircraft is published by Romeo et al. in 2010[14]. In 2011, 10 hours of flight endurance is achieved by the Faucon H2 UAV, from EnergyOr[4].

A fuel cell is an electro-chemical device that converts chemical energy into electrical energy and heat as a byproduct. The fuel cell will continuously deliver electric power as long as fuel is supplied. The most commonly used fuels are hydrogen and oxygen. There are many types of fuel cells available today: such as proton exchange membrane fuel cells, alkaline fuel cells, phosphoric acid fuel cells, solid oxide fuel cells, and molten carbonate fuel cells[18, 19]. In this paper, Polymer Electrolyte Membrane or Proton Exchange Membrane fuel cells (PEMFCs) are used because of their comparatively high efficiency, high energy density, low working temperature ($30 - 100°C$), compactness, easy and safe operational modes, in addition of being available in the marketplace for a variety of different systems[7, 10]. Fuel cell powered systems generally have a high current and a low voltage. However, the stack output of the fuel cell is decided by the numbers of the cells in the stack and is usually not a standard voltage. Fuel cell stacks are also sensitive to sudden changes in the loads; i.e. when the load increases, the fuel cell stacks voltage will drop steeply, which will affect the output voltage. Therefore, a DC-DC buck converter is proposed to step-down the fuel cell stacks output voltage to a desired value. A PID controller is suggested for the DC-DC buck converter to ensure a constant output voltage and to reject the disturbance from load and fuel cells stacks.

Besides having inconstant voltage output when current changes, fuel cells have other disadvantages such as slow dynamic response time and relatively long warming up time before full power output is available[19]. On the other hand, the battery has a fast dynamic response time to fluctuations in a load, and has high power density therefore; one of the ideal power solutions for long endurance UAV flights is the hybrid solution between the PEMFCs and Lithium-ion batteries. Combining a fuel cell and a battery in one power supply allows exploitation of the advantages of both devices and undermines their disadvantages. Hence, a fuel cell stack, a pack of Lithium-ion batteries, and a DC-DC buck converter will constitute the fuel cell-battery hybrid system. Traditionally, ad-hoc methods have been used to choose PID parameters. These classical methods, while valuable in terms of providing some insight into the process of control design, can often be surpassed in effectiveness by more modern methods. In this work, multi-parameter optimization technique is used for tuning the gains of the PID controller. This decreases the time and effort for tuning parameters considerably and proves that the day of ad-hoc methods for tuning PID controllers is ending[22].

The paper is organized in six sections: Section 2 describes briefly the components of the fuel cell-battery hybrid system. Section 3 details the operational characteristics and the mathematical modeling of the PEMFC, the Lithium-ion battery, and the DC-DC buck converter. In Section 4, the whole system is implemented in the Simulink environment, and a description of the UAV's mission scenario is presented. The design of the buck converter controller is detailed and the simulation results are explained in Section 5. Finally, the paper concludes with a brief summary in Section 6.

2 Hybrid system description

Fig. 1 shows the proposed fuel cell-battery hybrid power system. It consists of a PEMFC as a primary power source and a pack of Lithium-ion batteries as a second power source. A DC-DC buck converter is

used to step down the voltage to power: (i) a continuous load; a BLDC motor which represents the propulsive electric motor and (ii) suddenly changing loads; such as camera and servos.

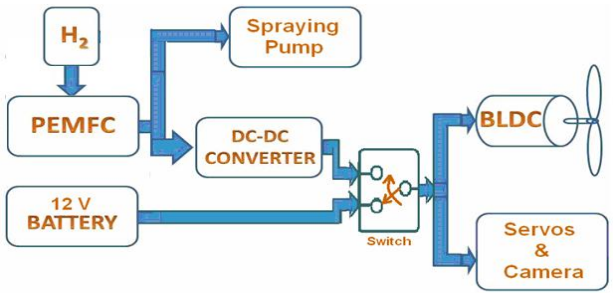

Fig. 1. Hybrid fuel cell-battery hybrid power system

A spray pump is directly powered from the PEMFC for aerial crop spraying. A controller is designed for the DC-DC buck converter to maintain the output voltage constant under sudden changes in the loads.

3 System modelling

3.1 Polymer electrolyte proton exchange membrane fuel cell

A PEMFC consists of a solid polymer electrolyte membrane sandwiched between two electrodes (anode and cathode), as shown in Fig. 2. When the hydrogen is injected at the anode and enters the electrolyte, it ionizes[19].
Anode:

$$H_2 \rightarrow 2H^+ + 2e^-. \tag{1}$$

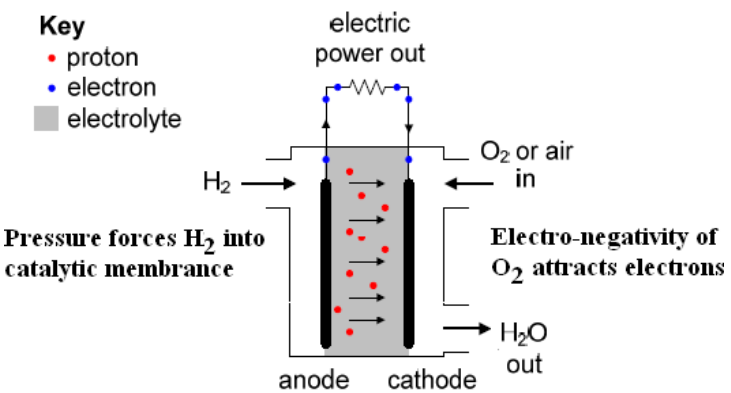

Fig. 2. Single PEMFC

Only protons are allowed to pass through the electrolyte, therefore the protons move across the electrolyte to the cathode to rejoin with oxygen, while the freed electrons from the hydrogen atoms travel through an external circuit to recombine with oxygen at the cathode.
Cathode:

$$O_2 + 4H^+ + 4e^- \rightarrow 2H_2O. \tag{2}$$

Therefore, the overall chemical reaction becomes:

$$2H_2 + O_2 \rightarrow 2H_2O + \text{Electricity} + \text{heat}, \tag{3}$$

i.e., hydrogen gas is recombined with oxygen gas producing electricity with water vapor as emission. A closed loop system could be operated whereby the water from of the PEMFC can be electrolyzed into oxygen and hydrogen for later re-use. Oxygen is generally obtained from the surrounding air.

Typically, a single fuel cell, as in Fig. 2, produces voltage between 0 and 1V based on the polarization $I - V$ curve; shown in Fig. 3, which expresses the relationship between output voltage and load current[23].

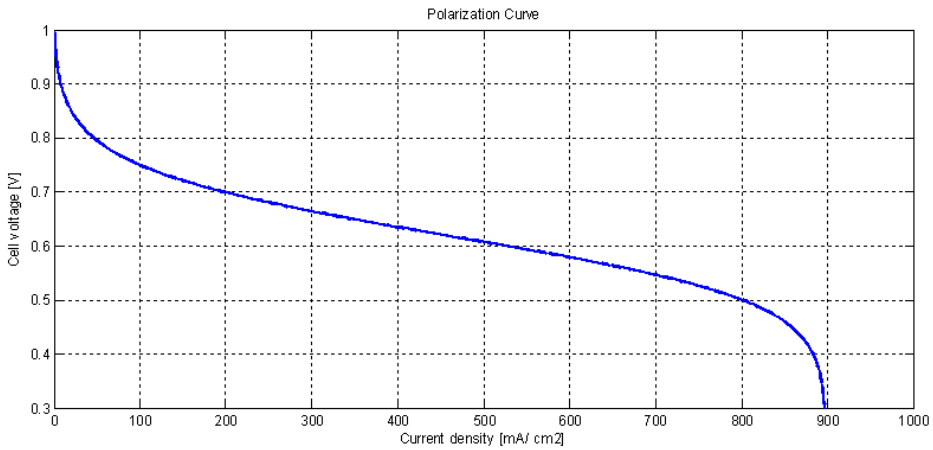

Fig. 3. Polarization curve

This relation can be written as Eq. (4)[21]. To produce a higher voltage, multiple cells have to be connected in series to build a fuel cell stack. Fig. 4 shows our fuel cell stack, which comprises 24 cells; the parameters of each are listed in Tab. 1.

$$V = E - \underbrace{(i + i_n)r}_{\text{Ohmic loss}} - \underbrace{A \ln\left(\frac{i + i_n}{i_0}\right)}_{\text{Activation loss}} + \underbrace{B \ln\left(1 - \frac{i + i_n}{i_l}\right)}_{\text{Concertation loss}}. \tag{4}$$

Table 1. Single PEMFC parameters

Parameter	Value
Open circuit voltage E	1.2 volt
Internal current density i_n	2 mA/cm^2
Internal resistance r	0.00003 k$\Omega.cm^2$
Activation losses constant A	0.06 volt
Exchange current density i_0	0.067 mA/cm^2
Concentration losses constant B	0.05 volt
Limit current density i_l	900 mA/cm^2

3.2 Lithium-ion battery

For the purpose of long endurance flight, another energy storage device is needed besides the main source; PEMFC, batteries are considered the most common choice in hybrid applications.

There are many types of batteries such as: Lead-acid, Nickel-metal-hydride, Sodium Sulfur, and Lithium-ion. In UAV applications, some features must be taken into consideration, via, (i) high specific power, (ii) high specific energy, and (iii) cycle life. A comparison among these types of batteries is made for such features[11].

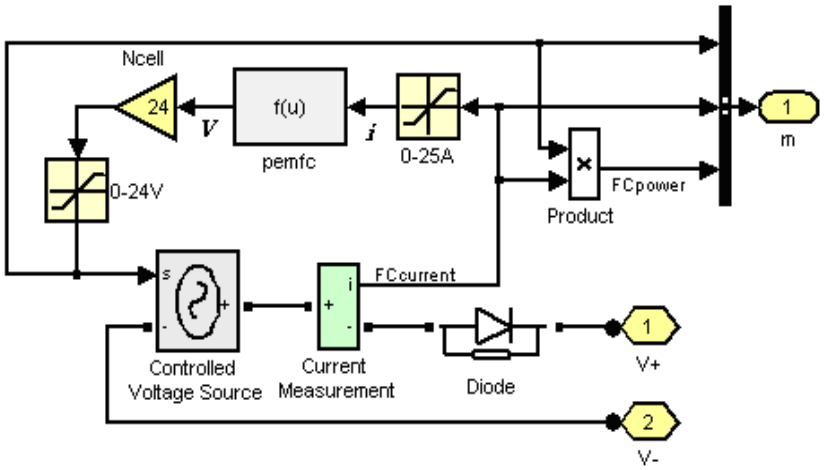

Fig. 4. Simulink model of PEMFC stack

Table 2. Comparison of the battery types

Battery type	Specific power $[W/Kg]$	Specific energy $[Wh/Kg]$	Energy efficiency	Cycle life
Lead-acid	150-400	35-50	80	500-1000
Nickel-Metal-Hydride	200-400	60-80	70	1000-2000
Sodium Sulfur	230	150-240	85	1000
Lithium-ion	200-350	90-160	> 90	> 1000

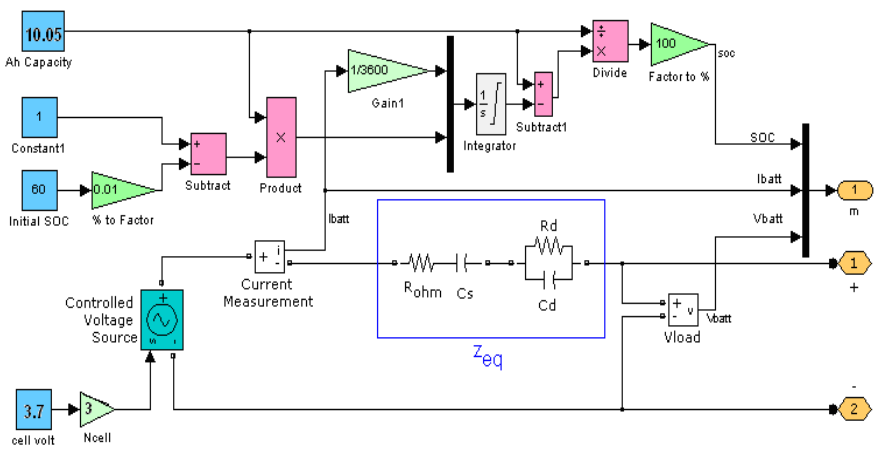

Fig. 5. Lithium-ion battery model

Tab. 2 shows that Lithium-ion battery fulfills all the requirements, which make it the suitable choice for electric-powered UAVs.

Lithium-ion battery model is introduced in Fig. 5 based on its output voltage (V_{batt}) and state-of-charge equations. The output voltage is expressed as:

$$V_{batt} = V_{OC} - I_{batt} \times Z_{eq}, \tag{5}$$

where V_{OC} and I_{batt} are the battery open circuit voltage and current, respectively. Z_{eq} is the battery equivalent internal impedance.

The cell state-of-charge (SOC) is defined as the amount of charge stored within the cell at any instant in time[20] . The SOC of the battery pack is calculated from the initial state of charge as:

$$SOC(t) = SOC_{\text{int ial}} - \frac{1}{Q}\int_{t_0}^{t} i_{\text{calc}}(t)dt, \tag{6}$$

where

SOC(t)	the Instantaneous battery SOC (%);
$SOC_{initial}$	the Initial battery SOC (%), at time = t_0;
$(t - t_0)$	the time interval under consideration (sec);
Q	time independent between open-circuit voltage and SOC.

The parameters of a Lithium-ion battery cell (model no.:BP2546) are shown in Tab. 3[16].

Table 3. Parameters of Lithium-ion battery

Parameter	Value
Nominal voltage	$3.7V$
Rated capacity	$3350mAh$
Charge voltage	$4.2V$

3.3 Buck converter

Buck converter is a type of switching-mode power supply which is used for stepping-down DC voltage level. It uses two switches (a MOSFET and a diode), an inductor and a capacitor. In Fig. 6, when a positive signal is applied at the MOSFET gate ($g > 0$), the DC input voltage V_{in} from the PEMFC/battery is allowed to charge the inductor and to supply output voltage V_{out} across the output capacitor C_{out}. Charging will continue till V_{out} reaches to reference voltage V_{ref}, then the control part turns OFF the switch ($g = 0$). The inductor will then change its voltage polarity and the current will flow in the same direction through the diode which is turned ON by switch controller part. Discharging will continue until V_{out} reaches below V_{ref}, then control part again turns ON the MOSFET to compensate V_{out} drop and this cycle continues until complete regulation of V_{out}[15]. This process is accomplished by sensing the output voltage of the circuit by means of a negative feedback loop to the PWM generator which controls the ON and OFF states of the MOSFET switches.

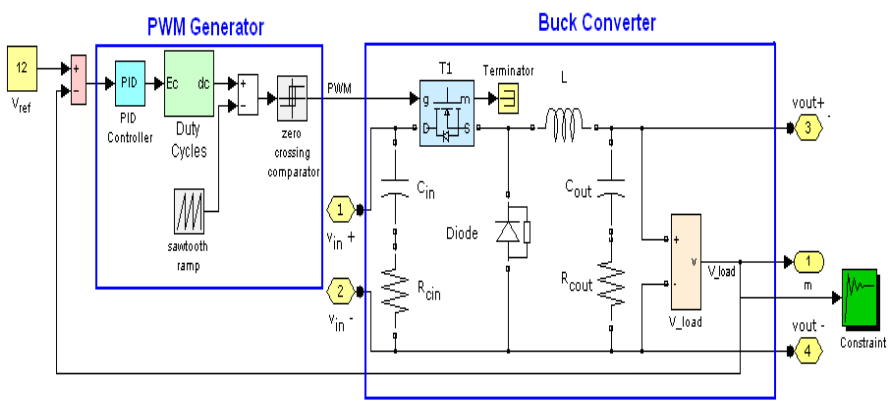

Fig. 6. Buck converter control loop

Controlling the switches, or in other words changing the duty cycle D to keep V_{out} equal to V_{ref} can be explained as follows: the error voltage ($V_E = V_{ref} - V_{out}$) is compared to sawtooth ramp V_{saw} generated by ramp generator, if voltage V_E is higher than V_{saw} as in Fig. 7, the PWM generator reduces the duty cycle by holding ON the MOSFET gate for a short time of every cycle. While V_E is lower than V_{saw}, the PWM generator increases the duty cycle by holding ON the gate for the most of cycle to rectify the output voltage.

The duty cycle is the ratio of the output voltage to the input voltage considering the voltage applied on diode V_F and MOSFET V_{out} as shown in Eq. (7), and it has a value in the interval 0 to 1.

$$D = \frac{V_{out} + V_F}{V_{in} - V_{R_{\text{DSon}}}}. \tag{7}$$

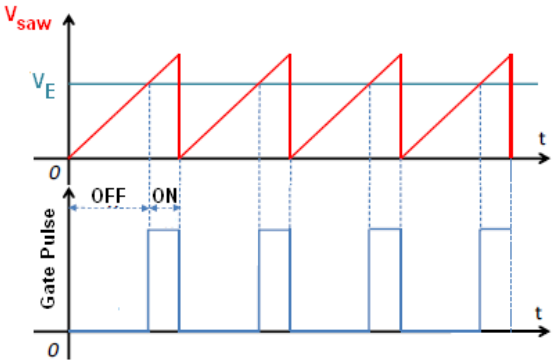

Fig. 7. PWM controlled input voltage

The selection criterion of the buck converter elements is explained as follows: the output capacitor (C_{out}) is chosen to filter the switching ripple; its capacitance must be large enough so that its impedance is much smaller than the load at the switching frequency, allowing most of the ripple current to flow through the capacitor, not the load. The output capacitor's equivalent series resistance $R_{C_{out}}$ must also be taken into account because its parasitic resistance causes additional voltage ripple[6]. The output voltage ripple V_{ripple} and the minimum output current $I_{\min}$ are assumed to be 1% of V_{out} and 10% of I_{out}, respectively:

$$C_{out} \geq C_{out\,\min} \qquad C_{out\,\min} = \frac{2I_{\min} \times T}{8V_{\text{ripple}}}. \tag{8}$$

The input capacitor (C_{in}) deals with highest ripple current. An acceptable level of the input voltage ripple $V_{\text{ripple}IN}$ is assumed to be 5% of V_{in}.

$$C_{in} \geq C_{in\,\min} \qquad C_{in\,\min} = \frac{I_{\text{peak}} \times T}{8V_{\text{ripple}IN}} = \frac{I_{\text{peak}} \times T}{8 \times (0.05 \times V_{in})}. \tag{9}$$

The minimum inductor value ($L_{\min}$) is calculated as follows:

$$L \geq L_{\min} \qquad L_{\min} = \frac{(V_{in} - V_{out} - V_{R_{\text{DSon}}}) \times T_{on}}{2 \times I_{\min}}. \tag{10}$$

According to the above equations, the calculated buck converter parameters are listed in Tab. 4.

4 System integration and mission scenario

The sub-systems are integrated in the Simulink environment as shown in Fig. 8. The UAV's mission involves several flying modes such as take-off, climbing, cruising, steady-state turning, descent and landing as shown in Fig. 9. At start-up process, the Lithium-ion battery is used to supply the power to the propulsive electric motor due to its fast dynamic response time of milliseconds. Then after 30 sec, the hydrogen fuel pump is switched ON to supply the fuel to the fuel cells, which in turn take about 30 seconds for the fuel cell reactions and the stack heating to reach power at maximum efficiency and hence the battery is switched OFF. The UAV's mission begins with the take-off and climbing modes; using the elevator control surface, and lasts until the desired altitude is achieved. Then the UAV starts to fly horizontally towards the target destination using both the ailerons and rudder control surfaces.

After flying 9 min, the camera is switched ON to assure reaching the desired waypoint, followed with crop spraying using the spray pump for about 45 min. After finishing its mission, the UAV returns back to reach the landing site again using both the ailerons and rudder control surfaces, followed by descending mode using the elevator control surface.

The amounts of power consumed by the loads vary according to their resistant loads. Tab. 5 summarizes the scenario of UAV's mission and illustrates the resistant loads of the propulsive BLDC motor[9], the control surfaces actuators and other loads.

Table 4. Buck converter parameters

Parameter	Symbol	Value	Unit	Parameter	Symbol	Value	Unit
Output voltage of converter	V_{out}	12	V	Duty cycle	D	0.496	
Input voltage of converter	V_{in}	26	V	Switching period	T	20	μsec
Nominal output current	I_{out}	2	A	On-time of the switch	T_{on}	9.922	μsec
Peak switching current	I_{peak}	2.2	A	Inductor value used	L	5650	μH
Maximum allowable peak-to-peak ripple	V_{ripple}	0.12	V	Output bank capacitance	C_{out}	166.67	μF
Drain to source resistance at switching on	R_{DSon}	0.1	Ω	Internal resistance of (C_{out}) used	$R_{C_{out}}$	0.015	Ω
Forward voltage drop across diode	V_F	0.8	V	Capacitance of input bank	C_{in}	500	μF
Voltage drop across R_{DSon}	$V_{R_{\text{DSon}}}$	0.2	V	Internal resistance of (C_{in}) used	$R_{C_{in}}$	0.1	Ω

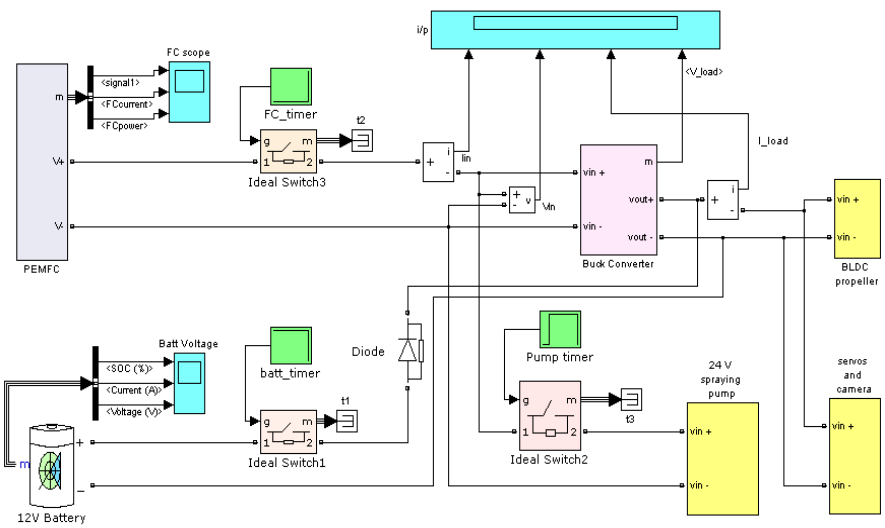

Fig. 8. Hybrid system Simulink model

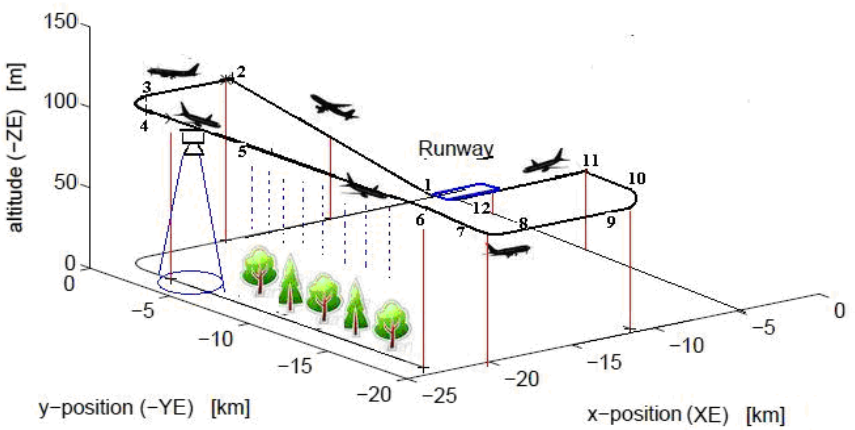

Fig. 9. UAV mission scenario

Table 5. Scenario of UAV's mission

Process	Time interval [min]	Description	Source	Loads
1	0-1	Start up Battery ON	Battery via buck	BLDC 13Ω
2	1-1.15	Battery OFF	Fuel cell via buck	BLDC 13Ω
3	1.15-3	Climbing	Fuel cell via buck	BLDC 13Ω+ elevator 30Ω
4	3-6	Horizontal flight	Fuel cell via buck	BLDC 13Ω
5	6-6.5	Turning	Fuel cell via buck	BLDC 13Ω+ailerons 30Ω+rudder 30Ω
6	6.5-9	Horizontal flight	Fuel cell via buck	BLDC 13Ω
7	9-9.5	Picturing	Fuel cell via buck	BLDC 13Ω+camera 14Ω
8	9.5-10	Horizontal flight	Fuel cell via buck	BLDC 13Ω
9	10-55	Crop spraying	Fuel cell via buck Fuel cell directly	BLDC 13Ω + spray pump 20Ω
10	55-59	Horizontal flight	Fuel cell via buck	BLDC 13Ω
11	59-60	Turning	Fuel cell via buck	BLDC 13Ω+ailerons 30Ω+rudder 30Ω
12	60-75	Horizontal flight	Fuel cell via buck	BLDC 13Ω
13	75-76	Turning	Fuel cell via buck	BLDC 13Ω+ailerons 30Ω+rudder 30Ω
14	76-80	Horizontal flight	Fuel cell via buck	BLDC 13Ω
15	80-82	Descending	Fuel cell via buck	BLDC 13Ω + elevator 30Ω

5 Buck converter controller design and simulation results

Controller design has centered mainly on simple, linear, proportional-integral-derivative (PID) controller. Although a PID controller is one of the earlier control strategies, it still has a wide range of applications in industrial control due to its easily implementation in the field environment.

A mathematical description of the PID controller is:

$$u(t) = K_p e(t) + K_i \int_0^t e(\tau)d\tau + K_d \frac{de(t)}{dt}, \tag{11}$$

where $u(t)$ is the input signal to the plant model, the error signal $e(t)$ is defined as $e(t) = r(t) - y(t)$, $y(t)$ is the output signal, and $r(t)$ is the reference input signal. K_p, K_i and K_d are the proportional, integral, and derivative gains, respectively.

Simulink Response Optimization Software (SROS) provides a GUI to assist in design of control and physical systems. With this product, optimization methods are used to adjust parameters within a nonlinear Simulink model to meet time-domain performance requirements by graphically placing constraints within a time-domain window and closely matching a reference signal[1].

Prior to the beginning of the optimization using SROS for the nonlinear system, the Signal Constraint block was connected to the V_load signal as in Fig. 6, where time domain constraints were placed graphically. The upper and lower constraint bounds in the Signal Constraint window were adjusted to ± 0.18; i.e., the

output voltage signal was required to track the reference signal; 12V, within maximum absolute error of 0.18. For optimization method, the algorithm used was the gradient descent.

By starting the optimization, the SROS automatically converts the time domain constraints into a constrained optimization problem, and then solves the problem using the gradient descend method. The constrained optimization problem formulated by SROS iteratively calls for simulations of the nonlinear system, compares the results of the simulations with the constraint objectives, and uses gradient methods to adjust tuned PID gains to better meet the objectives.

After few iterations, an optimal and feasible solution was found. The obtained PID gains were 7.342, 29.5784, and 0.0087 related to K_p, K_i and K_d, respectively. The simulation results for the whole hybrid system; Fig. 8, are given in Figs. 10, 11, 12, 13.

When system starts, the PEMFC gives no output current (see Fig. 13), therefore the propulsive BLDC motor is started using the battery only. One minute later, the fuel cell became capable of feeding the whole system thus the battery is disconnected. During horizontal flight as shown in Figs. 10 and 11, the BLDC motor; the only load, is powered via the buck converter, the load output current drawn is 0.92A and the output voltage is 12V.

It is obvious from Fig. 11 that the converter output current depends on the loads inserted to the system. When a sudden change occurred in the elevator actuator, the output current increased immediately to 1.32A and the output voltage decreased to 11.74V. Once this change is stopped, the output current is decreased and it is only needed to meet the requirement of the BLDC motor. When the load changed to two actuators; ailerons and rudder, the output current jumped to 1.72A. Similarly, using the camera raised the output current to 1.78A.

Since the spraying pump is powered directly from the fuel cell, therefore using the spraying pump in the interval [10:55] min affects the fuel cell output voltage and current as shown in Figs. 12 and 13.

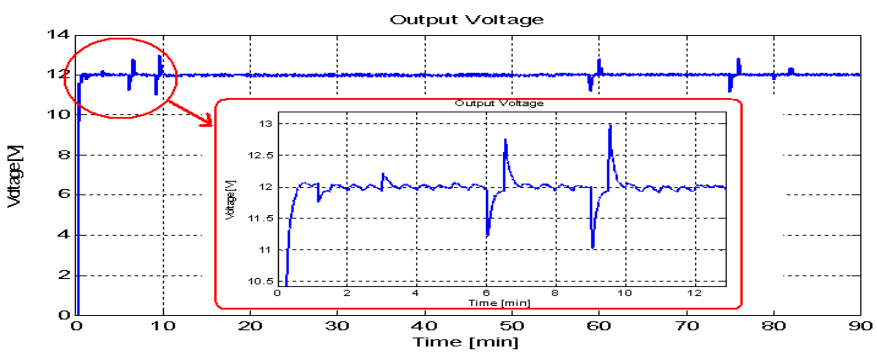

Fig. 10. Load output voltage

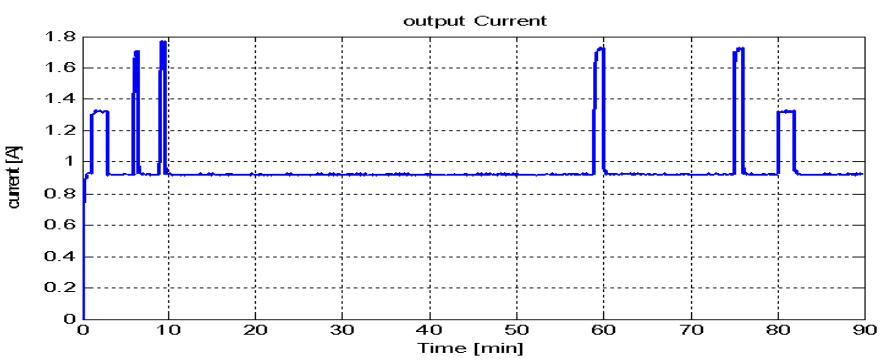

Fig. 11. Load output current

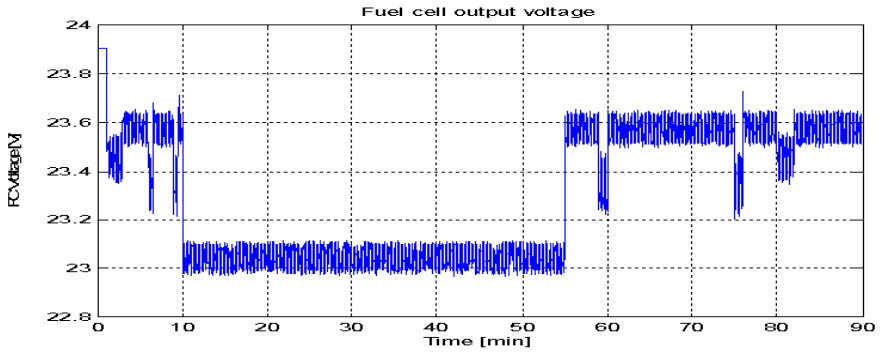

Fig. 12. PEMFC output voltage

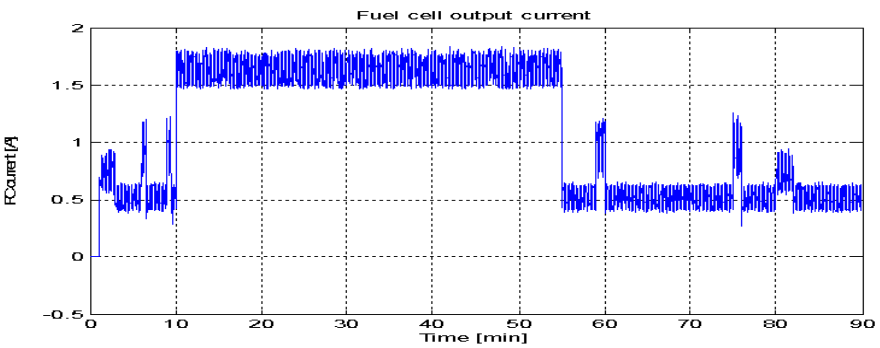

Fig. 13. PEMFC output current

6 Conclusions

Because of the limited flight endurance of electric UAVs that are powered by only batteries, this paper presented the development of a power management system for long endurance hybrid fuel cell and battery powered UAV propulsion application. As the main part of the development, a DC-DC buck converter for the fuel cell was built and the selection criterion of its elements was explained. For controlling the buck converter, a PID controller tuned by the gradient descend multi-parameter-optimization technique was designed. The proposed system was modeled and simulated using MATLAB/Simulink software. Simulation results verified the capability of the designed system to maintain the output voltage constant under sudden changes in the loads. Several advantages are gained on solving parameter optimization problems using computers; neither reliance on intuition nor experience in control is required, in addition to producing a satisfactory system response with optimal use of effort and time.

References

[1] Estimate and optimize simulink model parameters. mathworks. http://www.mathworks.com/products/sl-designoptimization.

[2] Nrl's ion tiger sets 26-hour flight endurance record. http://www.nrl.navy.mil/media/news-releases/2009/nrls-ion-tiger-sets-26hour-flight-endurance-record, 2009.

[3] Worlds first commercial fuel cell unmanned aerial system. http://www.gizmag.com/worlds-first-commercial-fuel-cell-unmanned-aerial-system/12453/, 2009.

[4] Energy or demonstrates fuel cell technology with defence research & development canada. 2011.

[5] T. Bradley, B. Moffitt, et al. Design space exploration of small-scale PEM fuel cell long endurance aircraft. **in:** *6th AIAA Aviation Technology Integration and Operations Conference*, 2006, **7701**: 2006.

[6] Buck Calculator. Texas instruments. http://focus.ti.com/download/aap/utilities/buck.xls.

[7] M. Dudek, P. Tomczyk, et al. Hybrid fuel cell-battery system as main power unit. *International Journal of Electrochemical Science*, 2013, **8**: 8442–8463.

[8] J. Freeh, J. Berton, et al. An analytical performance assessment of a fuel cell powered small electric airplane. *Electrical Systems Analysis at NASA Glenn Research Center: Status and Prospects*, 2003, **212393**: 14–15.
[9] Moog Components Group. Miniature brushless DC motors: DBH-0472 motor datasheet, 2006.
[10] L. Karunarathne. *An Intelligent Power Management System for Unmanned Aerial Vehicle Propulsion Applications*. Ph.D. Thesis, Cranfield University, 2012.
[11] S. Mantravadi. *Modeling, simulation and implementation of Li-ion battery powered electric and plug-in hybrid vehicles*. Master's Thesis, University of Akron, 2011.
[12] J. Meyer, F. Plessis, et al. *Aerial Vehicles: Design considerations for long endurance unmanned aerial vehicles*. Intech, 2009.
[13] Uninhabited air vehicles enabling science for military systems. *Committee on Materials, Structures, and Aeronautics Uninhabited Air Vehicles*, 2000.
[14] G. Romeo, F. Borello. Design and realization of a two-seater aircraft powered by fuel cell electric propulsion. *The Aeronautical Journal*, 2010, **114**(281-297).
[15] N. Safari. *Design of a DC/DC buck converter for ultra-low power applications in 65nm CMOS Process*. Master's Thesis, Linköping University, Sweden, 2012.
[16] Electronic Components Datasheets Search. Panasonic battery group. http://www.alldatasheet.com/datasheet-pdf/pdf/597043/PANASONICBATTERY/NCR18650B.html.
[17] A. Sehra, W. Whitlow. Propulsion and power for 21st century aviation. *Progress in Aerospace Sciences*, 2004, 14–42.
[18] EG&G Services. *Incorporation Fuel Cell Handbook*, Science Applications International Corporation, 2004.
[19] R. Smith. *Design of a control strategy for a fuel cell-battery hybrid power supply*. Master's Thesis, Texas A & M University, USA, 2009.
[20] B. Xiao, Y. Shi. A universal state-of-charge algorithm for batteries. **in:** *47th Design Automation Conference*, 2010, 687–692.
[21] Y. Xiao, K. Agbossou. Interface design and software development for pem fuel cell modeling based on matlab/simulink environment. *World Congress on Software Engineering*, 2009, **4**: 318–322.
[22] A. Youssef. Optimized pid tracking controller for piezoelectric hysteretic actuator model. *World Journal of Modelling and Simulation*, 2013, **9**: 223-234.
[23] Z. Zhang, W. Lee, et al. Pem fuel cell and battery hybrid power supply system design based on fuel flow rate control. **in:** *4th International Conference on Electric Utility Deregulation and Restructuring and Power Technologies*, 2011, 284–291.